Available online at www.sciencedirect.com
ScienceDirect
Journal of the European Ceramic Society 28 (2008) 995–1002
www.elsevier.com/locate/jeurceramsoc

Density functional study of structures and mechanical properties of Y-doped α-SiAlONs

L. Benco [a,b,*], J. Hafner [a], Z. Lences [b], P. Sajgalik [b]

[a] *Fakultät für Physik and Center for Computational Materials Science, Universität Wien, Sensengasse 8, A-1090 Wien, Austria*
[b] *Institute of Inorganic Chemistry, Slovak Academy of Sciences, Dubravska cesta 9, SK-84536 Bratislava, Slovak Republic*

Available online 24 October 2007

Abstract

A $2 \times 2 \times 1$ supercell of α-Si_3N_4 is used to model Y-doped α-SiAlON's (silicoalumino oxonitrides). Ab initio total energy calculations are performed at the DFT (GGA) level. A full relaxation of atomic positions is performed for stoichiometric α-Si_3N_4 and for a series of substituted structures with concentrations of Y, Al and O increasing up to the composition $Y_{0.5}Si_{9.5}Al_{2.5}O_{1.0}N_{15.0}$, similar to the observed solubility limits. The avoidance of neighboring AlX_4 (X = N,O) tetrahedra in highly doped structures indicates that the distribution of Al atoms in the framework of α-SiAlON's obeys the same Loewenstein rule as in aluminosilicate zeolite structures. An increase of the lattice parameters and cell volumes is observed with increasing degree of the doping. Changes are more pronounced for the insertion of Y than for Si-N/Al-O substitution. An introduction of a Y^{3+} cation into the interstitial position in the cage, however, causes a local contraction of the structure. Via the contraction a more efficient Y–N bonding is formed, leading to the stabilization of the Y-doped structure. The pronounced increase of the cell volume and the lattice parameters with Y-doping is due to three framework Al/Si framework substitutions compensating the extraframework Y^{3+} cation. The calculated bulk modulus (B_0) ranges from 223 GPa for pure α-Si_3N_4 to 197 GPa for $Y_{0.5}Si_{9.5}Al_{2.5}O_{1.0}N_{15.0}$. The slope of the decrease of B_0 with the degree of doping depends on the Y-content. For constant concentration of Y an increasing content of O causes a linear decrease of B_0.

Keywords: Y-doped α-SiAlONs; Density functional theory simulations; Electronic structure; Mechanical properties

1. Introduction

The properties of mixed silicoalumino oxonitrides with the structure of α-Si_3N_4 (known as α-SiAlON's), stabilized by doping with extraframework Y^{3+} cations have been extensively studied since their invention in the end of 1980s.[1–5] Needle-like microstructures and increased fracture toughness, compared to β-SiAlON materials, caused an increasing interest focused on the Y-stabilized α-phase.[6,7] Because single crystals are difficult to synthesize available structural data on Y-α-SiAlON's originate from powder structure refinements.[8–10] The structures of α-SiAlON's are complex and not precisely determined, because the random distribution of O and N leads to fluctuating bond lengths. Recently Ching et al. used accurate ab initio total-energy relaxations to determine the atomic positions of four known crystalline Y-Si-N-O phases[11] and compared structures and properties of 10 binary, ternary and quaternary crystals within the equilibrium phase diagram of the SiO_2-Y_2O_3-Si_3N_4 system.[12] Structure and bonding in spinel SiAlON's derived from the cubic *c*-Si_3N_4 have been analyzed theoretically by Ouyang and Ching[13] and Lowther et al.[14] First principles calculation of Ca-doped α- and β-SiAlON's has been reported by Fang and Metselaar.[15] Molecular-orbital calculations of La-α-SiAlON's and correlations to solubility and solution effects were published by Nakayasu et al.[16] The distribution of O and N atoms observed experimentally in β-SiAlON's were investigated by Fang and Metselaar[17] using first principles calculations.

In spite of the huge number of experimental investigations no first principles study of the structures of Y-α-SiAlON's has been reported so far. In this work we extend our previous study of the electronic structure and bulk properties of β-SiAlON's[18] to Y-doped α-Si_3N_4 and α-SiAlON's. A series of representative Y- and O-doped structures is constructed with increasing degree of doping with Y and O up to the solubility limit. For each structure

* Corresponding author at: Fakultät für Physik and Center for Computational Materials Science, Universität Wien, Sensengasse 8, A-1090 Wien, Austria. Fax: +43 1 4277 9514.
E-mail address: lubomir.benco@univie.ac.at (L. Benco).

0955-2219/$ – see front matter © 2007 Elsevier Ltd. All rights reserved.
doi:10.1016/j.jeurceramsoc.2007.09.030

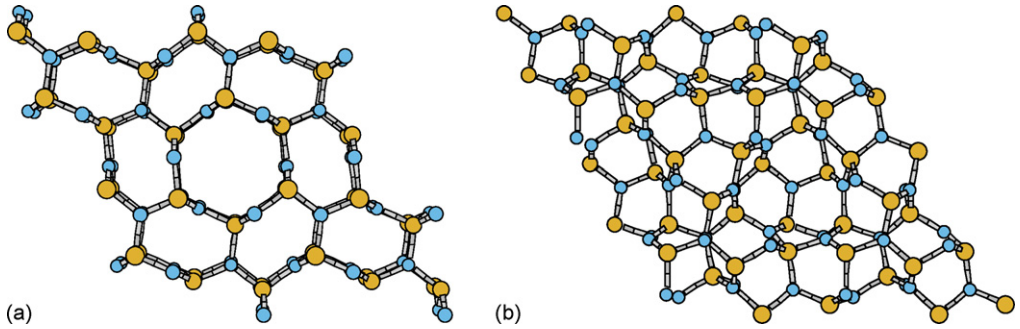

Fig. 1. Structure of β-Si_3N_4 (a) and α-Si_3N_4 (b). View along the *c* vector. Large circles, Si on tetrahedral sites; small circles, N on tri-coordinated sites.

the changes in equilibrium cell volume, lattice parameters and bulk modulus are evaluated and compared with stoichiometric α-Si_3N_4.

2. Structures

Fig. 1 compares the structures of β- and α-Si_3N_4. The structure of β-Si_3N_4 has space group $P6_3/m$ with two formula units per unit cell. Of the 14 atoms, seven are in plane A ($z = 0.25$), the other seven in plane B ($z = 0.75$), and the crystal consists of an ABAB stacking of layers of silicon and nitrogen atoms. The Si atoms are located on Wyckoff positions 6h in distorted SiN_4 tetrahedra. Nitrogen atoms at the corners of the tetrahedra (Wyckoff positions 2c and 6h) link three SiN_4 tetrahedra, forming continuous channels circumscribed by buckled rings with four or six tetrahedral sites, extending parallel to the *c* vector (Fig. 1a). The experimental cell parameters are $a = 7.595$ Å and $c = 2.902$ Å.[19] The structure of α-Si_3N_4 (space group $P3_1c$) exhibits ABCD stacking of atomic layers. The AB layer is the same in the α and β phases and the CD layer in the α phase is related to the AB layer by a *c*-glide plane. The unit cell is approximately twice as long in the *c* direction compared to β-Si_3N_4 ($a = 7.765$ Å and $c = 5.627$ Å),[19] it contains four formula units. The continuous channels fall into pieces, forming cages with a diameter equal to that of the channels (Fig. 1b).

In model structures of α-SiAlON's the Al/Si substitutions are distributed over the Si_3N_4 framework at large distances to avoid neighboring AlX_4 tetrahedra (X = N, O). The Y^{3+} cations are placed in an extraframework position in the center of the cage, a single atom compensates the charge of three framework Al/Si substitutions. Framework Y/Si substitutions are not considered. The highest Y- and Al-content observed by Hampshire[20] in Y-doped α-SiAlON's is $Y_{0.6}Si_{9.2}Al_{2.8}O_{1.1}N_{14.9}$. The degree of doping in the structures investigated in this work covers the entire range of solubility of Y and Al in α-SiAlON's. One Y^{3+} cation per primitive cell of α-Si_3N_4 leads to the composition $YSi_{9.0}Al_{3.0}N_{16.0}$ with a much higher Y-concentration than in real samples.[20] For the simulation of α-SiAlON materials with a realistic composition a $2 \times 2 \times 1$ supercell of α-Si_3N_4 is used. Both the primitive cell and the $2 \times 2 \times 1$ supercell are displayed in Fig. 2.

The solubility limit of Y in α-SiAlON materials corresponds to two ($Y^{3+} + 3Al/3Si$) substitutions per $2 \times 2 \times 1$ supercell producing the composition $Y_{0.5}Si_{10.5}Al_{1.5}N_{16.0}$. The

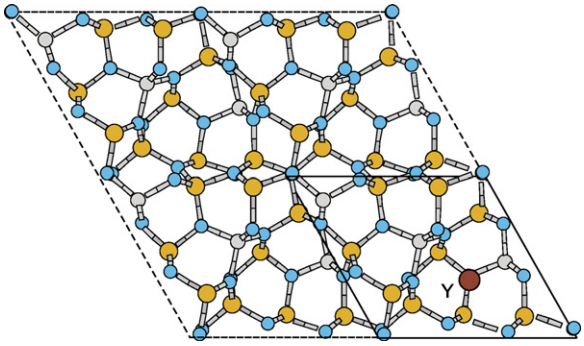

Fig. 2. Primitive unit cell of α-Si_3N_4 (full lines) and $2 \times 2 \times 1$ supercell (dashed lines). View along the *c* vector. Symbols see Fig. 1.

experimental composition of Y- and Al-richest α-SiAlON of $Y_{0.6}Si_{9.2}Al_{2.8}O_{1.1}N_{14.9}$[20] indicates that besides the Y-substitutions four additional Si-N/Al-O substitutions take place. The compositions of a series of structures formed in the $2 \times 2 \times 1$ supercell of α-Si_3N_4 with extraframework one and two Y atoms (Y = 1, 2) and up to four additional Al-O pairs (Al-O = 1 to 4) are collected in Table 1. The composition of the Y- and Al-richest experimental sample is given for comparison. An interesting observation is that even in the Y- and Al-richest structure with the composition $Y_{0.5}Si_{9.5}Al_{2.5}O_{1.0}N_{15.0}$ the distribution of Al over the tetrahedral sites still obeys the rule of avoiding neighboring AlX_4 (X = N,O) tetrahedra while at the same time all such sites are occupied. This suggests that the solubility of Al in α-SiAlON's is limited by a rule analogous to the Loewenstein rule[21] prohibiting in aluminosilicate zeolite struc-

Table 1
Y-doped and Si-N/Al-O substituted structures formed in the $2 \times 2 \times 1$ supercell of α-Si_3N_4 compared with Y- and Al-richest sample

Y atoms	Al-O pairs	*m*, *n*	$Y_{m/3}Si_{12-m-n}Al_{m+n}O_nN_{16-n}$
0	0	0, 0	α-Si_3N_4
1	0	0.75, 0	$Y_{0.25}Si_{11.25}Al_{0.75}N_{16.0}$
1	1	0.75, 0.25	$Y_{0.25}Si_{11.0}Al_{1.0}O_{0.25}N_{15.75}$
1	2	0.75, 0.5	$Y_{0.25}Si_{10.75}Al_{1.25}O_{0.5}N_{15.5}$
2	0	1.5, 0	$Y_{0.5}Si_{10.5}Al_{1.5}N_{16.0}$
2	1	1.5, 0.25	$Y_{0.5}Si_{10.25}Al_{1.75}O_{0.25}N_{15.75}$
2	2	1.5, 0.5	$Y_{0.5}Si_{10.0}Al_{2.0}O_{0.5}N_{15.5}$
2	3	1.5, 0.75	$Y_{0.5}Si_{9.75}Al_{2.25}O_{0.75}N_{15.25}$
2	4	1.5, 1.0	$Y_{0.5}Si_{9.5}Al_{2.5}O_{1.0}N_{15.0}$
Y- and Al-rich sample[20]		1.8, 1.1	$Y_{0.6}Si_{9.2}Al_{2.8}O_{1.1}N_{14.9}$

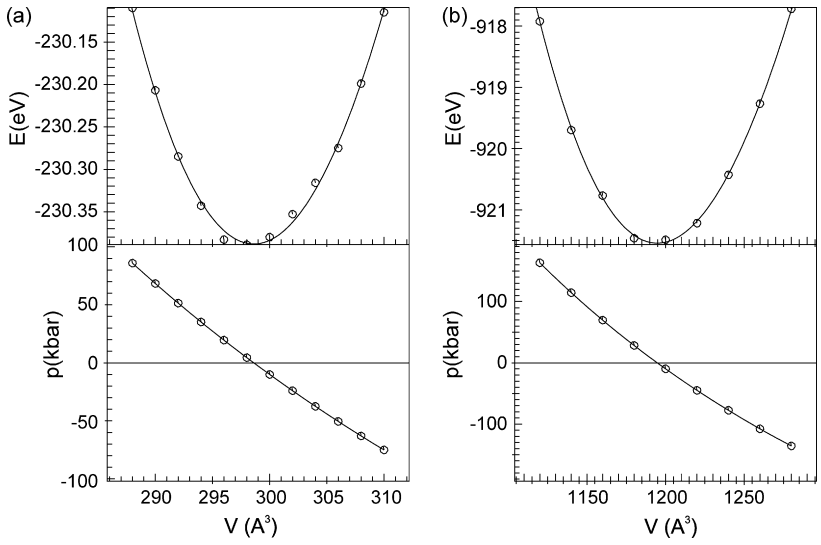

Fig. 3. Dependence of the total energy on the cell volume of α-Si_3N_4. (a) Primitive unit cell and (b) 2 × 2 × 1 supercell.

tures the occupation of two neighboring tetrahedral sites by Al atoms.

3. Computational method

Structure optimizations were performed for stoichiometric α-Si_3N_4 and for a series of SiAlON structures using the ab initio total-energy program VASP[22,23] based on density functional theory (DFT). The electron-ion interaction is described by Vanderbilt ultra-soft pseudo-potentials[24,25] and the projector augmented wave method.[26,27] The Kohn–Sham orbitals are expanded in plane waves with a kinetic energy cutoff of 400 eV. Electron exchange and correlation are treated in the generalized gradient approximation (GGA) as parametrized by Perdew and Wang (PW91).[28] The Brillouin-zone (BZ) is sampled on 12 points for stoichiometric α-Si_3N_4. Supercell calculations of Y-doped α-SiAlON's use a sampling based on two *k*-points only. A modest smearing of the eigenvalues close to the Fermi level is used to improve the convergence of the BZ integrations. Full relaxation of all the atomic positions is performed via a conjugate-gradient algorithm. The stopping criterion of the convergence procedure is a residual force acting on atoms smaller than 0.03 eV Å^3. In the fixed cell-volume relaxations of atomic positions no symmetry restrictions are applied.

4. Results

4.1. α-Si_3N_4

The total energy calculation allowing relaxation of all atomic positions is performed at different cell volumes with fixed cell-shape and a *c*/*a* ratio equal to the experimental value of 0.725. The dependence of the total energy on the cell volume of both the primitive cell and the 2 × 2 × 1 supercell of α-Si_3N_4 is displayed in Fig. 3. The fit using the Birch–Murnagham equation of state.[29]

$$E(\mathrm{V}) = E_0 + \left(\frac{B_0 V}{B_0'}\right)\left(\frac{(V_0/V)^{B_0'}}{B_0' - 1} + 1\right) - \frac{B_0 V_0}{B_0' - 1} \qquad (1)$$

provides the equilibrium cell volume V_0, the bulk modulus B_0 and its first pressure derivatives B_0' at zero pressure. The equilibrium cell volume of the primitive cell of 298.6 Å^3 is

Table 2
Lattice parameters and atomic coordinates of α-Si_3N_4

Property	This work	Experiment[30]
Lattice parameter *a* (Å)	7.8099	7.765
Lattice parameter *c* (Å)	5.6545	5.622
Cell volume (Å^3)	298.69	293.57
Internal parameters		
Si-1 (6c)		
x	0.5113	0.5130
y	0.4289	0.4305
z	0.6607	0.6580
Si-2 (6c)		
x	0.1676	0.1680
y	0.9143	0.9150
z	0.4525	0.4505
N-1 (6c)		
x	0.6112	0.6124
y	0.9552	0.9592
z	0.4334	0.4343
N-2 (6c)		
x	0.3193	0.3199
y	0.0037	0.0046
z	0.6988	0.7045
N-1 (2b)		
z	0.4536	0.4520
N-2 (2b)		
z	0.6059	0.6015

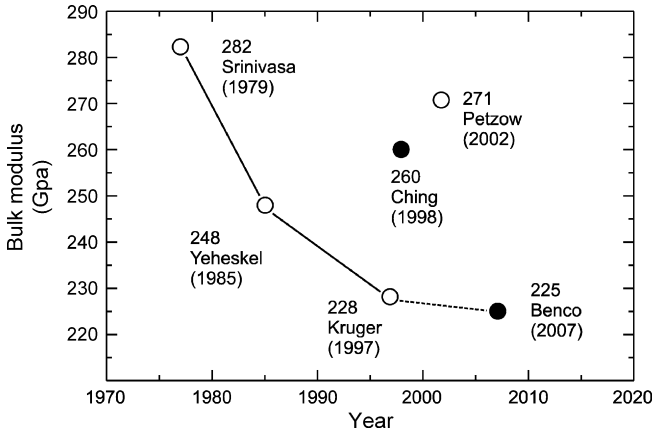

Fig. 4. Experimental (open circles) and calculated (full dots) bulk moduli of α-Si_3N_4. Experimental data according to Srinivasa et al.,[31] Yeheskel and Geten,[32] Kruger et al.,[33] Petzow and Herrmann,[34] LDA calculation by Ching et al.[35].

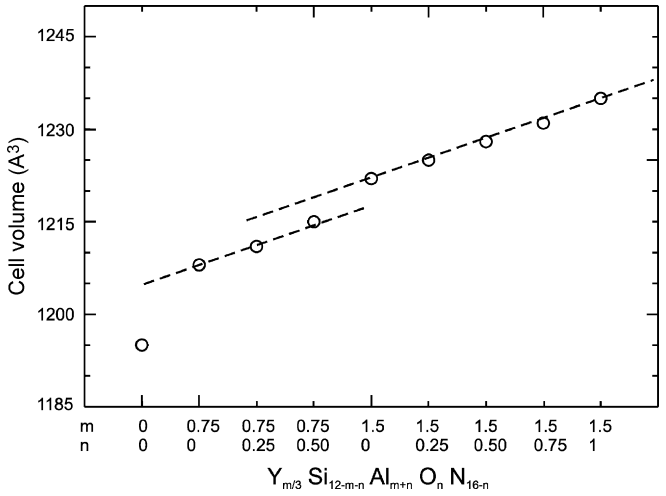

Fig. 5. Dependence of the cell volume of Y-doped α-SiAlON's with composition $Y_{m/3}Si_{12-m-n}Al_{m+n}O_nN_{16-n}$ (cf. Table 1) on the degree of doping. Dashed lines are guides to the eye.

nicely reproduced in the $2 \times 2 \times 1$ supercell calculation leading to 298.7 Å^3. The predicted cell volume overestimates the experimentally determined volume of 293.6 Å^3 by 1.7%. Atomic coordinates of α-Si_3N_4 calculated for the optimized cell volume are together with experimental coordinates collected in Table 2. The lattice parameters of the optimized cell are overestimated by 0.54%. Deviations of atomic coordinates are typically smaller than 0.5%. The largest deviation of 0.73% is observed for the z coordinate of the N atom in the Wyckoff position 2b for which the crystal symmetry fixes the x and y atomic coordinate.

The calculated bulk moduli for the primitive cell and for the $2 \times 2 \times 1$ supercell are 218 GPa and 225 GPa, respectively. Slightly different values are due to different precisions. For the smaller primitive cell a sampling in 12 k-points is used and k-space of the $2 \times 2 \times 1$ supercell is sampled in only two k-points. In Fig. 4 the bulk modulus calculated using the $2 \times 2 \times 1$ supercell is compared with available experimental and calculated data. The bulk modulus derived from measurements of the Young's modulus decreases from 282 GPa (Srinivasa et al.[31]), to 248 GPa (Yeheskel and Getel[32]), and to 228 GPa (Kruger et al.[33]). Except for the value of 271 GPa by Petzow and Herrmann[34] experimental moduli exhibit a systematic decrease of the measured value with the year of the measurement. The time evolution of the measured property indicates that mechanical properties of α-Si_3N_4 are sensitive to the admixture of the β-phase and with improving quality of measured samples the value of the bulk modulus exhibits a systematic decrease. Our calculated value of 225 GPa represents the lower limit to the bulk modulus of α-Si_3N_4. Another calculated value is 260 GPa. Ching et al.[35] used local density approximation leading systematically to shorter interatomic distances, stronger bonding and higher bulk moduli than the GGA.

4.2. Y- and O-doped α-SiAlONs

Because of the much larger covalent radius of the Al atom (118 pm) compared to the Si atom (111 pm) doping leads to an expansion of the unit cell. The variation of the cell volume in a series of Y-doped α-SiAlON's constructed in the $2 \times 2 \times 1$ supercell of α-Si_3N_4 with increasing degree of doping is listed in Table 3 and displayed in Fig. 5. Both types of substitutions, $Y^{3+} + 3Al/3Si$ and Al-O/Si-N, cause an expansion of the cell volume. A much larger change, however, is observed on insertion of a Y^{3+} cation. For a constant concentration of Y^{3+} the increase in O content leads to a linear increase of the cell volume as indicated by dashed lines for two different concentrations of the Y^{3+} cation. Table 3 presents also lattice parameters corresponding to the equilibrium cell volume at the particular degree

Table 3
Calculated lattice parameters (Å) and the cell volume (Å) of Y- and O-doped structures and lattice parameters from the fit of experimental data[36]

$Y_{m/3}Si_{12-m-n}Al_{m+n}O_nN_{16-n}$	m, n	DFT calculation (this work)			Equations by Sun et al.[36]	
		Cell volume	a	c	a	c
α-Si_3N_4	0, 0	1194.7	7.8075	5.6578	7.7520	5.6200
$Y_{0.25}Si_{11.25}Al_{0.75}N_{16.0}$	0.75, 0	1208.1	7.8366	5.6789	7.7858	5.6560
$Y_{0.25}Si_{11.0}Al_{1.0}O_{0.25}N_{15.75}$	0.75, 0.25	1211.5	7.8439	5.6842	7.7880	5.6583
$Y_{0.25}Si_{10.75}Al_{1.25}O_{0.5}N_{15.5}$	0.75, 0.5	1215.2	7.8519	5.6900	7.7903	5.6605
$Y_{0.5}Si_{10.5}Al_{1.5}N_{16.0}$	1.5, 0	1222.2	7.8669	5.7009	7.8195	5.6920
$Y_{0.5}Si_{10.25}Al_{1.75}O_{0.25}N_{15.75}$	1.5, 0.25	1225.0	7.8729	5.7052	7.8218	5.6943
$Y_{0.5}Si_{10.0}Al_{2.0}O_{0.5}N_{15.5}$	1.5, 0.5	1228.5	7.8804	5.7106	7.8240	5.6965
$Y_{0.5}Si_{9.75}Al_{2.25}O_{0.75}N_{15.25}$	1.5, 0.75	1231.2	7.8862	5.7148	7.8263	5.6988
$Y_{0.5}Si_{9.5}Al_{2.5}O_{1.0}N_{15.0}$	1.5, 1.0	1235.0	7.8943	5.7207	7.8285	5.7010

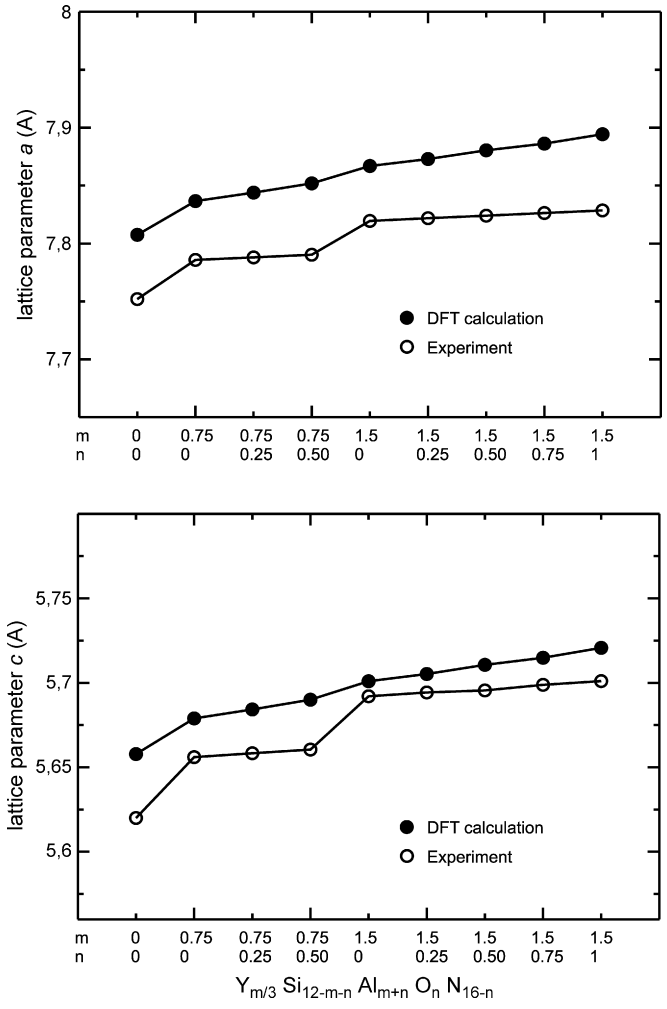

Fig. 6. The lattice parameters of Y- and O-doped α-SiAlON's.

of doping. For comparison, we quote also lattice parameters calculated according to empirical equations derived by Sun et al.[36] for Y-containing α-SiAlON's:

$$a_0(\text{Å}) = 7.752 + 0.045m + 0.009n, \quad (2)$$

$$c_0(\text{Å}) = 5.620 + 0.048m + 0.009n. \quad (3)$$

The lattice parameters are visualized in Fig. 6. Both calculated lattice parameters are slightly larger than the experimental values. This is a consequence of the use of the GGA approach to the functional for the exchange and correlation of electrons. While local density approximation (LDA) leads to too short lattice parameters, the semilocal GGA leads to slightly longer lattice vectors, usually closer to experimental values. Theory predicts a linear increase of the cell volume and lattice parameters with both the Y-concentration and the degree of Al-O/Si-N substitution, with a steeper slope of the former. The empirical relation of Sun et al.[35] provides a stronger dependence on the Y-content and only a very weak dependence on the degree of Al-O/Si-N substitution (Fig. 5).

Substitutions in the α-Si_3N_4 structure leading to the formation of α-SiAlON's cause both a local expansion and a local compression of the structure analogous to those observed in β-SiAlON's.[18] A local expansion occurs due to the Al/Si substitution in the tetrahedral site. The expansion of the tetrahedron induces a compression of bonds adjacent to the tetrahedron. Because of similar covalent radii the O/N substitution does not lead to pronounced changes of bond distances.[18] The variation of bond length with the degree of doping is illustrated by selected interatomic distances collected in Table 4. The extraframework Y^{3+} cation exhibits a tendency to attract framework O and N atoms. The bond lengths around atoms in a contact with the Y^{3+} cation are therefore considerably deformed. For Si–N and Al–N bonds Table 4 reports two different bond lengths. The first one is the length of a bond in the bulk and the second one is the length of a bond where the N atom is in contact with the interstitial Y^{3+} cation. In pure α-Si_3N_4 the Si–N bond length of 1.747 Å is similar to that in β-Si_3N_4 (1.746 Å).[18] With increasing doping rate the Si–N bond length elongates to ∼1.770 Å. The Si–N bonds with the N atom attracted towards the Y^{3+} cation are by approximately 6% longer. In the Y- and O-richest sample such a Si–N bond is elongated to ∼1.780 Å. Due to the larger covalent radius of the Al atom Al–N bonds are longer compared to Si–N bonds. In the Y- and O-richest sample the Al–N bond length extends to ∼1.796 Å and when the N atom is in contact with the Y^{3+} cation the Al–N bond length is stretched to 1.897 Å (cf. Table 4). A variation between 1.753 and 1.779 Å is observed for the Si–O bond length and between 1.906 and 1.926 Å for the Al–O bond length. The change of the bond length with the doping rate should be smooth and exhibit an incremental increase as observed in experiments. The irregularities observed for bonds reported in Table 4 are caused by the choice of a particular bond (Si–N, Al–N), whose length is influenced by other substitutions in close vicinity of the bond.

Table 4
Variation of selected interatomic distances (Å) with the degree of doping

$Y_{m/3}Si_{12-m-n}Al_{m+n}O_nN_{16-n}$	m, n	Si–N···Si	Si–N···Y	Al–N···Si	Al–N···Y	Y–N (av)	Y–N short	Si–O	Al–O
α-Si_3N_4	0, 0	1.747							
$Y_{0.25}Si_{11.25}Al_{0.75}N_{16.0}$	0.75, 0	1.754	1.765	1.785	1.883	2.568	2.269		
$Y_{0.25}Si_{11.0}Al_{1.0}O_{0.25}N_{15.75}$	0.75, 0.25	1.754	1.765	1.805	1.889	2.572	2.271	1.753	1.920
$Y_{0.25}Si_{10.75}Al_{1.25}O_{0.5}N_{15.5}$	0.75, 0.5	1.755	1.766	1.813	1.887	2.569	2.274	1.758	1.906
$Y_{0.5}Si_{10.5}Al_{1.5}N_{16.0}$	1.5, 0	1.765	1.769	1.794	1.889	2.570	2.276		
$Y_{0.5}Si_{10.25}Al_{1.75}O_{0.25}N_{15.75}$	1.5, 0.25	1.765	1.773	1.794	1.891	2.566	2.280	1.779	1.917
$Y_{0.5}Si_{10.0}Al_{2.0}O_{0.5}N_{15.5}$	1.5, 0.5	1.769	1.778	1.790	1.887	2.568	2.282	1.776	1.897
$Y_{0.5}Si_{9.75}Al_{2.25}O_{0.75}N_{15.25}$	1.5, 0.75	1.770	1.780	1.782	1.889	2.562	2.279	1.746	1.926
$Y_{0.5}Si_{9.5}Al_{2.5}O_{1.0}N_{15.0}$	1.5, 1.0	1.768	1.780	1.796	1.897	2.567	2.284	1.763	1.925

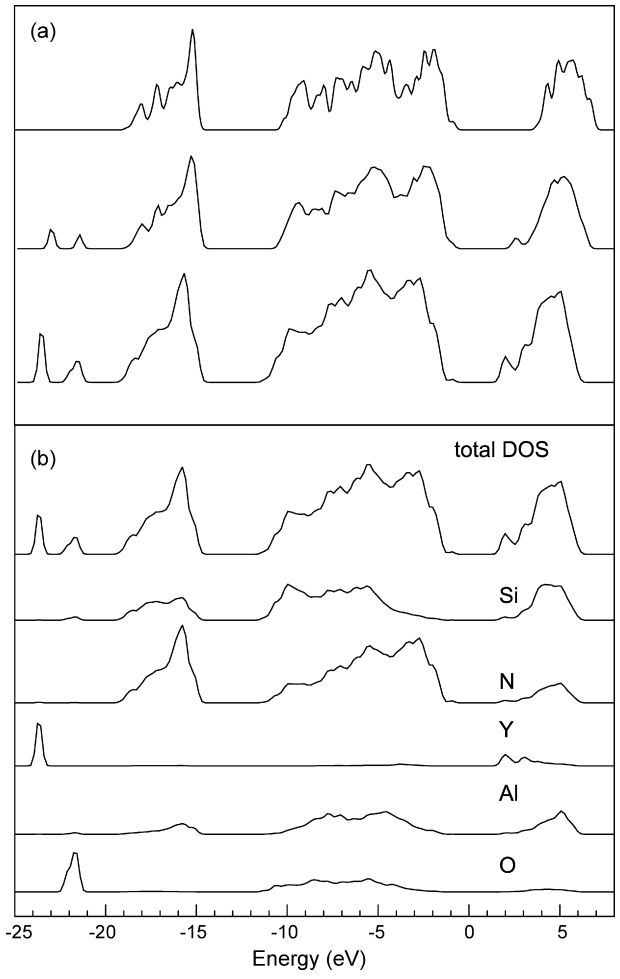

Fig. 7. Calculated total and partial DOS. (a) The total DOS of pure α-Si_3N_4 (top), medium-doped $Y_{0.25}Si_{10.75}Al_{1.25}O_{0.5}N_{15.5}$ (center) and high-doped $Y_{0.5}Si_{9.5}Al_{2.5}O_{1.0}N_{15.0}$ (bottom). (b) The total DOS (top) and atom-projected partial DOS of high-doped $Y_{0.5}Si_{9.5}Al_{2.5}O_{1.0}N_{15.0}$.

The Si–O and Al–O bond lengths listed in Table 4 are averaged. Because only small number of such bonds exist in the model structures under study, the statistics is naturally modest.

The calculated total and partial DOS are displayed in Fig. 7. The total DOS is compared for pure α-Si_3N_4, medium-doped $Y_{0.25}Si_{10.75}Al_{1.25}O_{0.5}N_{15.5}$, and high-doped $Y_{0.5}Si_{9.5}Al_{2.5}O_{1.0}N_{15.0}$ (Fig. 7a). The total DOS of α-Si_3N_4 consists of three bands composed of s-states, p-states and the band of empty states above the Fermi level (conduction band).[37] With increasing doping two narrow core-like bands grow at ∼−24 eV and ∼−23 eV. The p band only slightly broadens from ∼−10 eV to ∼−11 eV. Simultaneously with two core-like states a new band appears at the bottom-side of the conduction band, causing considerable narrowing of the band gap. In Fig. 7b the total DOS and atom-projected partial DOS are displayed for Y- and O-richest sample. The scale of low-concentration elements Y, Al and O is zoomed-in for clarity. The partial DOS show that core-like bands originate from Y 4p and O 2s states. The broadening of the p band is due to the admixture of the O 2p states. The new band in the band gap originates from Y 4d states. Doping with yttrium thus leads to a considerable change of electrical properties of the material.

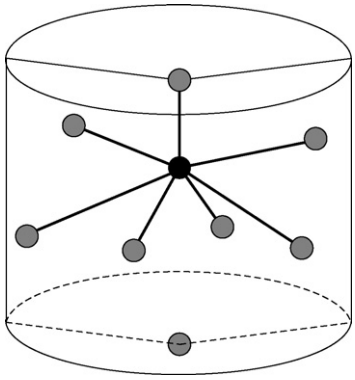

Fig. 8. Schematic display of the bonding of the Y^{3+} cation to framework atoms of α-SiAlON's. Black dot, Y; gray dots, N, or O.

The bonding of a Y^{3+} cation to framework atoms is schematically displayed in Fig. 8. In the cylindrical cage of α-SiAlON the extraframework Y^{3+} cation resides approximately on the central axis and forms both lateral and axial connections to N/O atoms of the framework. Six bonds are formed to atoms on the side wall of the cage. At a low degree of doping with the composition $Y_{0.25}Si_{11.25}Al_{0.75}N_{16.0}$ the six Y–N distances range from ∼2.48 Å to ∼2.68 Å, with an averaged value of 2.568 Å. With increasing rate of doping the average Y–N distance decreases from 2.568 Å (cf. Table 4) to 2.562 Å in Y-rich samples. The expansion of the cell volume (cf. Fig. 5) thus leads to a compression of the volume of the cage. The compression strengthens the Y–N bonds, leading to a stabilization of the Y-doped α-SiAlON structure. The Y–N distance of two axial N atoms equals to the *c* lattice vector of ∼5.68 (cf. Table 2). This distance is too large for the Y^{3+} cation to reside in the center of the cage and to form two equivalent axial Y–N bonds. The Y^{3+} cation is therefore off-centered and forms only one strong axial Y–N bond, considerably shorter than the lateral Y–N bonds. Because the base of the cage is slightly buckled the efficient Y–N bond is formed with the N atom shifted towards the center of the cage (cf. Fig. 8). With increased doping the axial Y–N distance increases from 2.269 to 2.284 Å (Table 4). This is in contrast to the shortening of the lateral Y–N distances. A compression of the volume of the cage leads to a more efficient Y–N bonding forming a more regular coordination sphere around the interstitial Y^{3+} cation. A more regular coordination sphere makes the Y^{3+} cation move from the off-centered position towards the center of the cage. This shift to a more central position of the Y^{3+} cation causes the increase of the axial Y–N distance.

The calculated bulk moduli of the series of Y- and O-doped α-SiAlON's are displayed in Fig. 9 and listed in Table 5. With increasing degree of doping the bulk modulus continuously decreases from 225 GPa for stoichiometric α-Si_3N_4 to 196 GPa for the Y- and O-richest α-SiAlON. The value of the bulk modulus of stoichiometric α-Si_3N_4 consistently fits the dependence. This is another piece of evidence that the calculated value of the bulk modulus of the stoichiometric α-Si_3N_4 is correct. The reason for a large scatter of experimental values (cf. Fig. 4) could

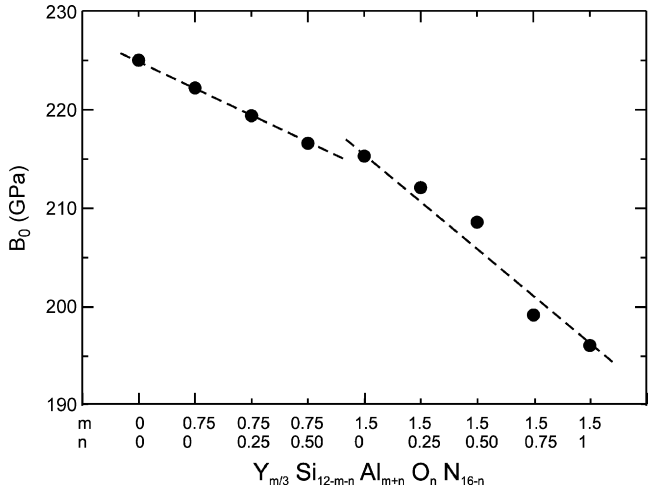

Fig. 9. Calculated bulk modulus of Y- and O-doped α-SiAlON's. Dashed lines are guide to the eye.

Table 5
Calculated bulk moduli B_0 of Y- and O-doped structures (GPa)

$Y_{m/3}Si_{12-m-n}Al_{m+n}O_nN_{16-n}$	m, n	B_0
α-Si_3N_4	0, 0	225
$Y_{0.25}Si_{11.25}Al_{0.75}N_{16.0}$	0.75, 0	222
$Y_{0.25}Si_{11.0}Al_{1.0}O_{0.25}N_{15.75}$	0.75, 0.25	219
$Y_{0.25}Si_{10.75}Al_{1.25}O_{0.5}N_{15.5}$	0.75, 0.5	216
$Y_{0.5}Si_{10.5}Al_{1.5}N_{16.0}$	1.5, 0	215
$Y_{0.5}Si1_{0.25}Al_{1.75}O_{0.25}N_{15.75}$	1.5, 0.25	212
$Y_{0.5}Si_{10.0}Al_{2.0}O_{0.5}N_{15.5}$	1.5, 0.5	209
$Y_{0.5}Si_{9.75}Al_{2.25}O_{0.75}N_{15.25}$	1.5, 0.75	199
$Y_{0.5}Si_{9.5}Al_{2.5}O_{1.0}N_{15.0}$	1.5, 1.0	196

be a different quality of samples and/or different conditions of the measurement. Because of two different concentrations of Y two dependences of the bulk modulus are observed. At higher content of Y the bulk modulus decreases more steeply and at constant concentration of Y an increased concentration of O leads to a linear decrease of the bulk modulus.

5. Conclusions

A model for the simulation of the properties of Y- and O-doped α-SiAlON's has been constructed. Using a $2 \times 2 \times 1$ supercell of α-Si_3N_4 eight structures are chosen to cover the entire range of stable compositions up to the limit of solubility of both Y and O. The construction of the Y- and O-rich structures shows that the distribution of the Al atoms in the framework obeys a rule analogous to Loewenstein's rule of avoiding AlX_4 tetrahedra (X = N, O).

Full relaxation of all atomic positions at different cell volumes, performed using ab initio density functional theory, and a Birch–Murnagham fit of the equation of state, provide the equilibrium cell volume, the lattice parameters, and bulk moduli of a series of α-SiAlON's with a degree of doping up to the solubility limits. The calculated lattice parameters are slightly larger than the experimental values, in accordance with typical GGA results. With the degree of doping an expansion of the cell volume is observed. Increasing O content leads to a linear increase of the cell volume and the lattice parameters. Much larger changes of lattice parameters, compared with the Si-N/Al-O substitution, are observed for the insertion of an extraframework Y^{3+} cation. The variation of bond lengths with the doping rate shows that the Y^{3+} cation itself leads to a local contraction of the structure and the increase of the cell volume and the lattice parameters is due to three Al/Si substitutions compensating the extraframework Y^{3+} cation.

The calculated bulk modulus of pure α-Si_3N_4 of 225 GPa represents a lower limit to the experimental data. With increasing degree of doping the bulk modulus decreases. For a constant concentration of Y a linear decrease of the bulk modulus with increasing O-content is observed. For a higher concentration of Y the dependence of the bulk modulus on the O-content becomes steeper. For the model structure close to Y- and O-richest α-SiAlON the bulk modulus exhibits the lowest value of 196 GPa.

Acknowledgments

This work has been supported by the Austrian Science Fund under project No. P17020-PHYS. Computational resources are partly granted by the Computing Center of Vienna University (Schrödinger II).

References

1. Hampshire, S., Park, H. K., Thompson, D. P. and Jack, K. H., α-Sialon ceramics. *Nature*, 1978, **274**, 880–883.
2. Mitomo, M., Tanaka, H., Muramatsu, K., Ii, N. and Fujii, Y., The strength of α-sialon ceramics. *J. Mater. Sci.*, 1980, **15**, 2661–2662.
3. Mitomo, M., Izumi, F., Bando, Y. and Sekikawa, Y., Characterization of α-sialon ceramics. In *Ceramic Components for Engines*, ed. S. Somiya *et al.* KTK Science Publishers, Tokyo, Japan, 1984, pp. 377–386.
4. Ishizawa, K., Ayuzawa, N., Shiranita, A., Takai, M., Uchida, N. and Mitomo, M., Some properties of α-sialon ceramics. In *Ceramic Materials and Components for Engines*, ed. W. Bunk and H. Hausner. German Ceramic Society, Bad Honnef, Germany, 1986, pp. 511–518.
5. Stutz, D., Greil, P. and Petzow, G., Two-dimensional solid-solution forming of Y-containing α-Si_3N_4. *J. Mater. Sci. Lett.*, 1986, **5**, 335–336.
6. Slasor, S. and Thompson, D. P., Comments on two-dimensional solid-solutions forming of Y-containing a-Si3N4. *J. Mater. Sci. Lett.*, 1987, **6**, 315–316.
7. Chen, I-. W. and Rosenflanz, A., A tough SiAlON ceramic based on α-Si_3N_4 with a whisker-like microstructure. *Nature*, 1997, **389**, 701–704.
8. Izumi, F., Mitomo, M. and Bando, Y., Rietveld refinment for calcium and yttrium containing α-sialons. *J. Mater. Sci.*, 1984, **19**, 3115–3120.
9. Cao, G. Z., Metselaar, R. and Haije, W. G., Neutron diffraction study of yttrium α'-sialon. *J. Mater. Sci. Lett.*, 1993, **12**, 459–460.
10. Smrcok, L., Salamon, D., Scholtzova, E. and Richardson Jr., J. W., Time-of-flight Rietveld neutron structure refinement and quantum chemistry study of Y-α-sialon. *J. Eur. Ceram. Soc.*, 2006, **26**, 3925–3931.
11. Ching, W. Y., Ouyang, L., Yao, H. and Xu, Y. N., Electronic structure and bonding in the Y-Si-O-N quaternary crystals. *Phys. Rev. B*, 2004, **70**. p. 085105-1–085105-14.
12. Ching, W. Y., Electronic structure and bonding of all crystalline phases in the Silica-Yttria-Silicon Nitride phase equilibrium diagram. *J. Am. Ceram. Soc.*, 2004, **87**, 1996–2013.
13. Ouyang, L. and Ching, W. Y., Structure and bonding in a cubic phase of SiAlON derived from the cubic spinel phase of Si_3N_4. *Appl. Phys. Lett.*, 2002, **81**, 229–231.

14. Lowther, J. E., Schwarz, M., Kroke, E. and Riedel, R., Electronic structure calculations of cohesive properties of some $Si_{6-z}Al_zO_zN_{8-z}$ spinels. *J. Solid State Chem.*, 2003, **176**, 549–555.
15. Fang, C. M. and Metselaar, R., First-principles calculations of the stability and local structure of α-sialon ceramics on the line Si_3N_4-1/2 Ca_3N_2:3AlN. *J. Phys. Condensed Matter*, 2004, **16**, 2931–2939.
16. Nakayasu, T., Yamada, T., Tanaka, I., Adachi, H. and Goto, S., Electronic structure of Ln^{3+} α-sialons with correlations to solubility and solution effects. *J. Am. Ceram. Soc.*, 1996, **79**, 2527–2532.
17. Fang, C. M. and Metselaar, R., First-principles calculations of microdomain models for β-sialon Si_5AlON_7. *J. Am. Ceram. Soc.*, 2003, **86**, 1956–1958.
18. Benco, L., Hafner, J., Lences, Z. and Sajgalik, P., Electronic structure and bulk properties of β-sialons. *J. Am. Ceram. Soc.*, 2003, **86**, 1162–1167.
19. Grun, R., The crystal structure of β-Si_3N_4: Structural and stability considerations between α- and β-Si_3N_4. *Acta. Crystallogr. B: Crystallogr. Cryst. Chem.*, 1979, **35**, 800–804.
20. Hampshire, S., Park, H. K., Thompson, D. P. and Jack, K. H., α′-Sialon Ceramics. *Nature*, 1978, **274**, 880–882.
21. Loewenstein, W., The distribution of aluminum in the tetrahedra of silicates and aluminosilicates. *Am. Miner.*, 1954, **39**, 92.
22. Kresse, G. and Hafner, J., Ab initio molecular dynamics for open-shell transition metals. *Phys. Rev. B*, 1993, **48**, 13115–13118.
23. Kresse, G. and Furthmuller, J., Efficient iterative scheme for ab initio total energy calculations using plane-wave basis set. *Comp. Mater. Sci.*, 1996, **6**, 16–50.
24. Vanderbilt, D., Soft self-consistent pseudopotentials in a generalized eigenvalue formalism. *Phys. Rev. B*, 1990, **41**, 7892.
25. Kresse, G. and Hafner, J., Normconserving and ultrasoft pseudopotentials for first-row transition elements. *J. Phys. Condensed Matter*, 1994, **6**, 8245.
26. Blochl, P. E., Projector augmentd-wave method. *Phys. Rev. B*, 1994, **50**, 17953.
27. Kresse, G. and Joubert, D., From ultrasoft pseudopotentials to the projector augmented-wave method. *Phys. Rev. B*, 1999, **59**, 1758.
28. Perdew, J. P., Chevary, A., Vosko, S. H., Jackson, K. A., Pedersen, M. R., Singh, D. J. *et al.*, Atoms, molecules, solids, and surfaces. Applications of the generalized gradient approximation for exchange and correlation. *Phys. Rev. B*, 1992, **46**, 6671.
29. Birch, F., Finite strain isotherm and velocities for single crystal and polycrystalline NaCl at high pressure at 300 K. *J. Geophys. Res. [Athmos.]*, 1978, **83**, 1257–1268.
30. Kohatsu, I. and McCauley, J. W., Re-examination of crystal structure of α-Si_3N_4. *Mater. Res. Bull.*, 1974, **9**, 917–920.
31. Srinivasa, S. R., Cartz, L., Jorgensen, J. D., Worlton, T. G., Beyerlein, R. and Billy, M., High-pressure neutron difraction study of Si_2N_2O. *J. Appl. Crystallogr.*, 1977, **10**, 16–71.
32. Yeheskel, O. and Gefen, Y., The effect of the α-phase on the elastic properties of Si_3N_4. *Mater. Sci. Eng.*, 1985, **71**, 95–99.
33. Kruger, M. B., Nguyen, J. H., Li, Y. M., Caldwell, W. A., Manghani, M. H. and Jeanloz, R., Equation of state of α-Si_3N_4. *Phys. Rev. B*, 1997, **55**, 3456–3460.
34. Petzow, G. and Herrmann, M., Silicon nitride ceramics. In *Structure and Bonding*, *vol. 102*. Springer Verlag, Berlin, 2002, pp. 50–166.
35. Ching, W. Y., Xu, Y. N., Gale, J. D. and Ruhle, M., Ab-initio total energy calculation of α- and β-silicon nitride and the derivation of effective pair potentials with application to lattice dynamics. *J. Am. Ceram. Soc.*, 1998, **81**, 3189–3196.
36. Sun, W. Y., Tien, T. Y. and Yen, T. S., Solubility limits od a'-SiAlON solid solutions in the system Si, Al, Y/N, O. *J. Am. Ceram. Soc.*, 1991, **74**, 2547–2550.
37. Xu, Y. N. and Ching, W. Y., Electronic structure and optical properties of α and β phases of silicon nitride, silicon oxynitride, and with comparison to silicon dioxide. *Phys. Rev. B*, 1995, **51**, 17379–17389.